

MSE-422 - Advanced Metallurgy**Exam 27/01/2023****09h15 – 10h45**

Family name: _____

First name: _____

No. Sciper: _____

Question	Points
1	/19
2	/20
3	/16
4	/20
Total:	/75
Grade:	

- Do not write more text than is necessary; sometimes, you can answer the questions with 1-2 words.
- You can also write on the backside of the sheets. If you do so, please indicate clearly to which question your answer belongs.
- If you need more paper for your answers, please ask.

1) Advanced steels & steel metallurgy (19P)

a) In the table below, several steels are listed with their EN steel name designation. Complete the table by adding the amount of each alloying element in wt.% (2P)

Table 1: Designations and compositions of four different steels

Nr	Steel	Cr	Ni	Mo	Mn	V	C	N
1	X90CrMoV 18-1-1							
2	X13CrMnMoN 18-14-3-1							
3	X3CrNiMo 25-7-4							
4	10CrMo9-10							

b) With the help of the Schaeffler diagram below, determine the phases that can be found in each steel. (2P)

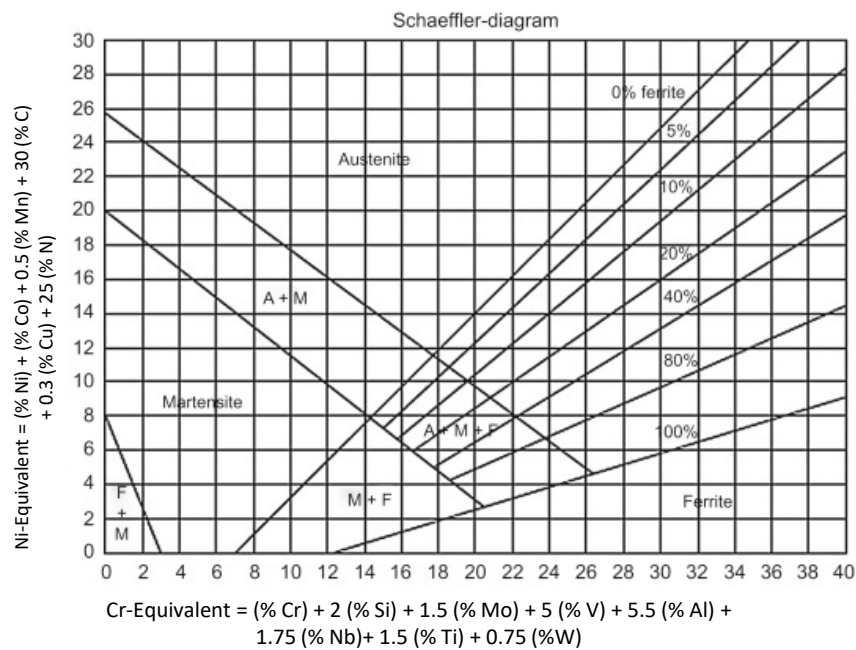


Figure 1: Schaeffler diagram;

Table 2: Designations and phases of four different steels;

Nr	Steel	Phases
1	X90CrMoV 18-1-1	
2	X13CrMnMoN 18-14-3-1	
3	X3CrNiMo 25-7-4	
4	10CrMo9-10	

c) Besides their role as ferrite stabilizers, briefly explain the general role of Cr and Mo in the above mentioned steels. (2P)

d) Which of the above mentioned steels would you use for the following applications? Justify your answer briefly.

- Sushi knife blades (2P)

- Temporary orthopedic implant for bone fixation (2P)

- f) Two steels with the compositions given in Table 3, were uniaxially deformed during tensile test until failure.

Table 3: Compositions of the two steels;

Steel	C	Si	Mn	P	Ni	Cr	Cu	N
Steel 1	0.15	0.45	11.09	0.041	1.97	13.36	0.04	0.18
Steel 2	0.08	0.47	11.04	0.042	1.18	15.93	0.03	0.2

The amount of martensite was measured during the tensile test at different strain levels and the values are plotted in Figure 2-a as a function of the applied strain. It can be seen that the amount of martensite is significantly higher in steel 2 than in steel 1. Figure 2-b shows the stress-strain curves for the two steels.

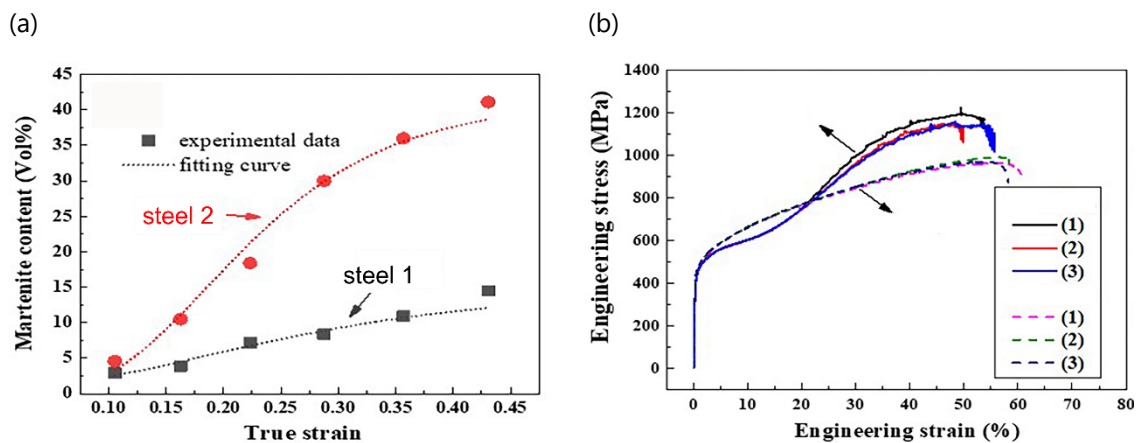


Figure 2: a) Evolution of the amount of martensite with the applied true strain; b) Engineering stress-strain curves of the steel 1 and steel 2;

- Explain the term 'stacking fault energy' (SFE)? What are the main factors affecting the SFE? (2P)
- Which of the two steels of the Table 3 and Figure 2 has the lower SFE? Justify your answer. (2P)

- Assign the name of the steels (steel 1 and steel 2) to the corresponding engineering stress-strain curves in Figure 2-b and justify your answer. (2P)

2) Ni-based high temperature alloys (20 P)

- a) Figure 3-a shows a single-crystalline (SX) turbine blade, which was made from the Ni-based superalloy CMSX-4 using the Bridgman furnace process (schematic Figure 3-b). During the casting process, the withdrawal velocity was set to 20 mm/min and the thermal gradient at the solid/liquid interface was set to 2500 K/m.

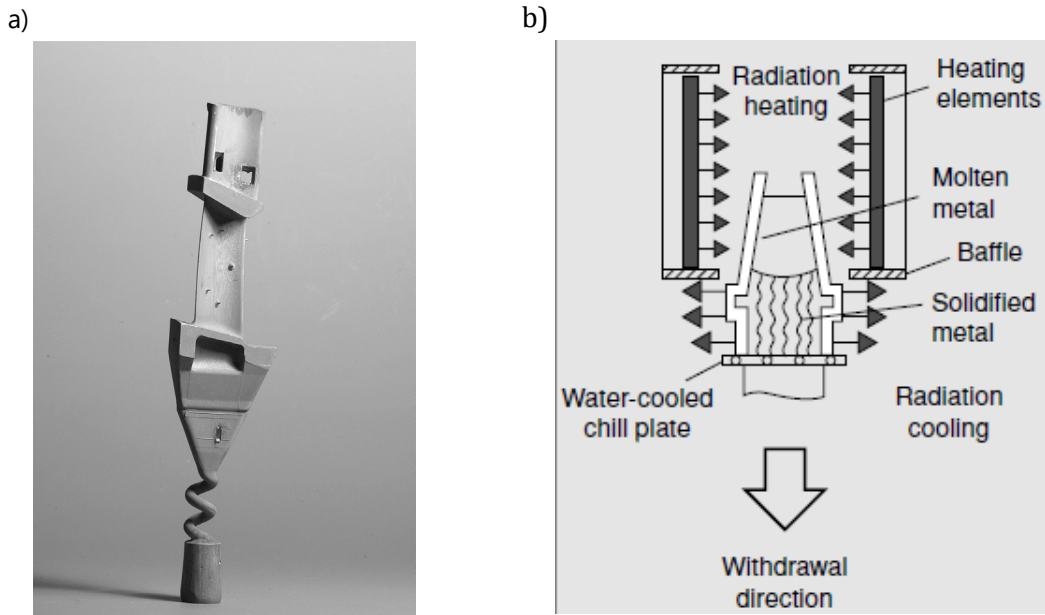


Figure 3: a) Single-crystalline turbine blade; b) schematic of the Bridgman furnace process;

- Explain the function of the 'pig-tail' in the lower part of the cast turbine blade. (1P)

- Name and briefly explain two typical casting defects that would occur when increasing the withdrawal velocity to 40 mm/min. (3P)

b) After casting, components fabricated from single-crystal superalloys undergo a complicated heat treatment designed to remove the microsegregation inherited from the casting process.

- Explain briefly why microsegregation occurs during casting of Ni superalloys. (2P)

- What would be the implications of not heat-treating the cast components? (2P)

- c) Creep samples from the single-crystal superalloys TMS-75 and TMS-82+ alloys were cast such that the compositions of the γ and γ' -Ni₃Al phases were on a common tie-line, so that the phase compositions remain invariant. The compositions of the two alloys (in wt.%) are given in Table 4. Figure 4 shows the creep rupture life of the two alloys as a function of the fraction of the γ' phase present at 900°C and at 1100°C.

Table 4: Chemical compositions of TMS-82+ and TMS-75 (in wt.-%);

Alloy	Co	Cr	Mo	W	Al	Ti	Ta	Hf	Re	Ni
TMS-82+	7.8	4.9	1.9	8.7	5.3	0.5	6.0	0.1	2.4	Bal.
TMS-75	12.0	3.0	2.0	6.0	6.0	-	6.0	0.1	5	Bal.

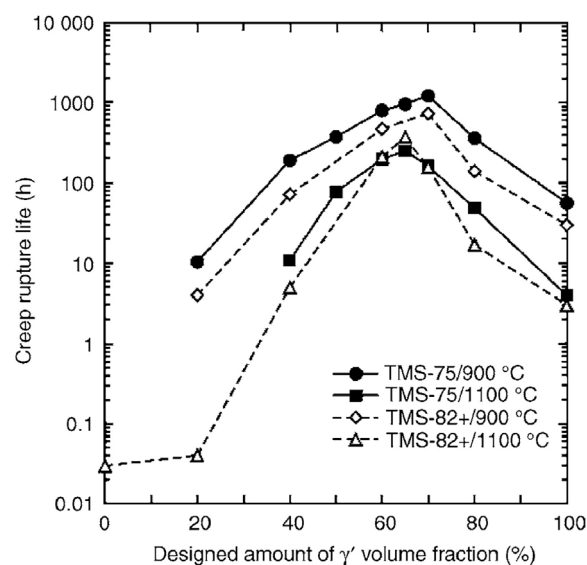


Figure 4: Creep rupture life of TMS-75 and TMS-82+ as a function of the fraction of the γ' phase ($\sigma = 392$ MPa @ $T = 900^\circ\text{C}$, $\sigma = 137$ MPa @ $T = 1100^\circ\text{C}$);

- Explain the general shape of the curves, i.e. the first increasing and then again decreasing creep rupture life with increasing γ' phase fraction. Why is the maximum creep resistance not imparted at a 50% fraction of γ' phase? (2P)
- Explain the in general higher creep rupture life of the TMS-75 alloy at γ' phase fractions below 60 vol% considering their chemical compositions. (2P)

d) Figure 5 shows the binary Ni-Al phase diagram.

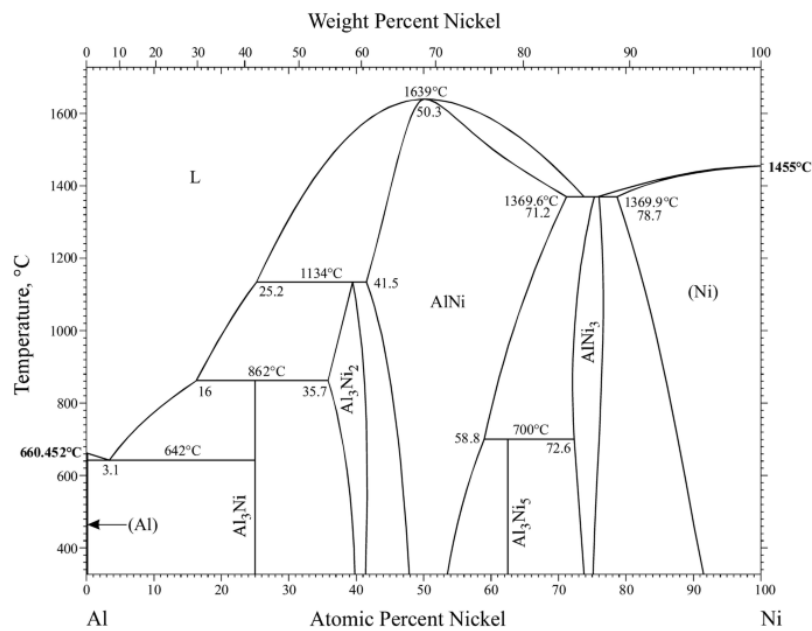


Figure 5: Binary Ni-Al diagram;

- Give two reasons why alloys with a composition of approximately 50 at.% Ni and 50 at.% Al are of interest as a replacement for Ni superalloys for high-temperature applications such as turbine blades. (2P)
- Is the phase NiAl a Laves phase? Justify your answer. (2P)

3) Al and Mg alloys (16P)

a) You have been given two alloys with the following designations: AA2024 (T6) and AZ31 (T4). Based on these information, please name:

- The category of alloys these materials belong to (2P)

- The main alloying elements and their impact (2P)

- The thermal treatment these alloys have been subjected to (2P)

b) You have been given the responsibility for the heat treatment of a AA6063 alloy containing 0.9 wt% Mg, 0.6 wt.% Si and minor amounts of Zn and Ti.

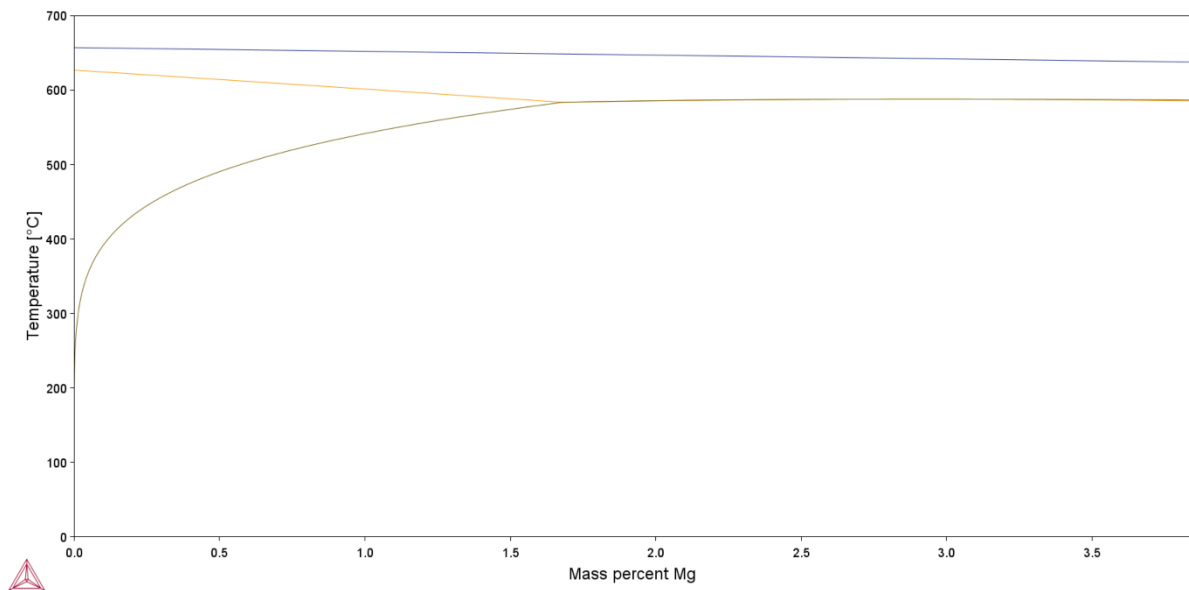


Figure 6: Quasi-binary $Al_{0.6}Si - Mg$ phase diagram;

- In Figure 6, the calculated Al-rich corner of the binary section of the Al-Mg-Si phase diagram at a fixed amount of Si of 0.6 wt.% is given. The phase diagram includes the liquid, the aluminium matrix (FCC) and the precipitation phase (Mg_2Si). Define the phase-fields on the given diagram. (2P)

4) Ti Alloys (20P)

a) In Ti alloys the addition of α stabilizers increases the α/β transformation temperature, whereas the addition of β stabilizers decreases the α/β transformation temperature.

- What are the lattice structures (names and sketches) of the α phase and of the β phase? (2P)

- *Figure 7* shows schematically the influence of α and β stabilizers on the phase fields in Ti alloys. Complete the graphs with two examples for α stabilizing and two examples for β stabilizing elements in Ti alloys. (2P)

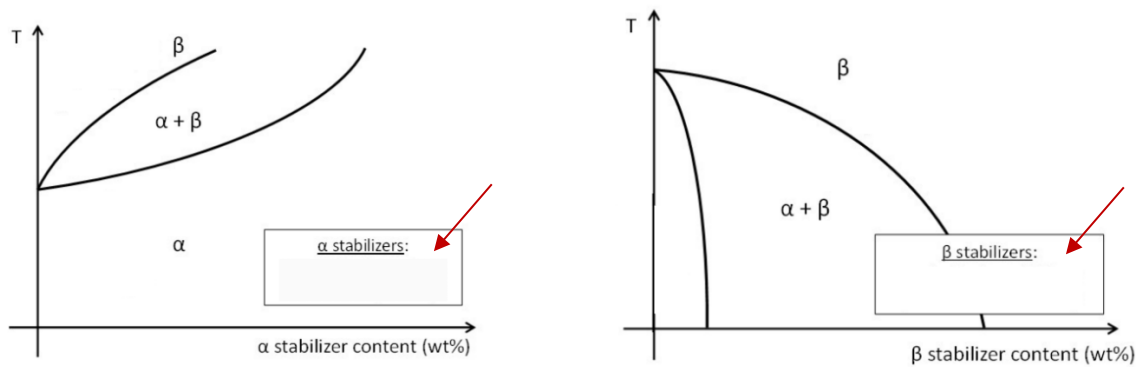


Figure 7: Influence of α and β stabilizers on the phase fields in Ti alloys;

- Based on their alloying elements (α stabilizers and β stabilizers), Ti alloys are classified as α -alloys, $\alpha + \beta$ alloys and β -alloys. Complete Table 5 defining to which class the following alloys belong to (compositions given in wt. %). (3P)

Table 5: Names and compositions (given in wt. %) of different Ti alloys;

Alloy class	Grade	Al	Sn	Zr	Mo	Ta	Nb	Fe	O
	Ti-5Al-2.5Sn	5	2.5	--	--				0.2
	Ti-6Al-2Sn-4Zr	6	2	4	--				0.2
	Ti-29Nb-13Ta	29	--	--	--	13	--	0.03	0.4
	Ti-6Al-7Nb	6	--	--	--	0.2	7	--	0.2
	Ti-15Mo-2.7Nb-0.2Si	--	--	--	15	--	2.7	0.1	0.1
	Ti-7Al-4Mo	7	--	--	4	--	--	--	0.1

- b) The compressor blades of an aero-engine are fabricated from the alloy Ti-6Al-4V. The compressor blades, after being manufactured by forging, show a bimodal microstructure that consist partly of equiaxed (primary) α in a lamellar $\alpha+\beta$ matrix. Once fabricated, the blades are welded using laser beam welding (LBW). Figure 8-a shows the geometry of the welding zone after the process. During LBW, the welded material experiences a particular thermal history, which affects the microstructure of the fabricated blades. The temperature in the weld pool was measure remotely at the position indicated by a red cross in Figure 8-b. Figure 8-a shows the evolution of the temperature recorded by the thermocouple during the laser beam welding of the parts (red curve).

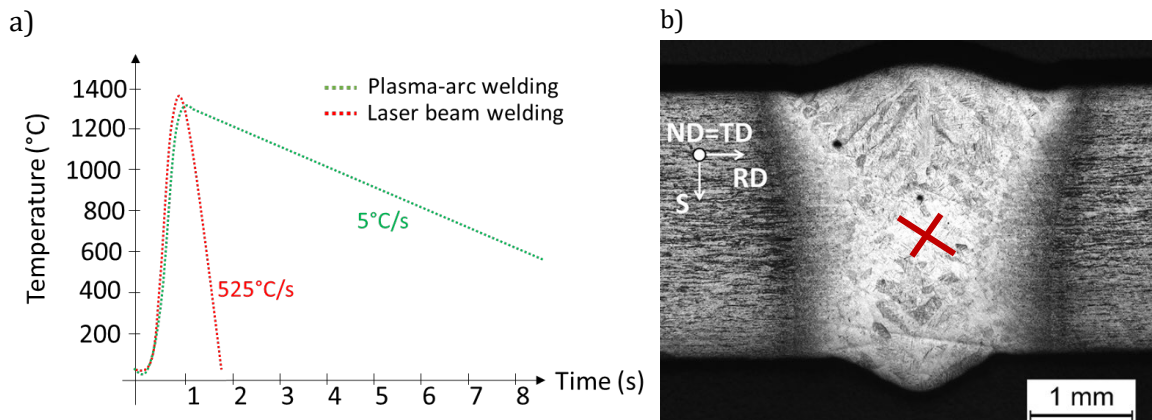
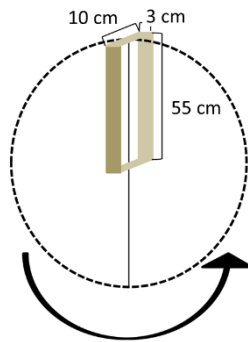


Figure 8: a) Temperature evolution measured by thermocouple at the center of the weld during laser beam welding (red curve) and during plasma-arc welding (green curve); b) geometry of the welding zone;

- Which type of microstructure do you expect to form at the center of the weld after laser beam welding? (Phase or phases, grain size) (2P)
- How does the microstructure of the welding zone change if the same blades are welded by plasma-arc welding? Consider the thermal history experienced by the welded material reported in Figure 8-a). (2P)

- c) The blades have a density of 4.4 g/cm^3 . The blade dimensions are $55 \times 10 \times 3 \text{ cm}^3$ and rotate with an angular velocity (ω) of 6275 rpm (Figure 9). The S-N curves have been determined using rotating loading and were designed in a way to simulate as closely as possible the service condition of the blades. (NB: considering a point mass located at the extremity of the blade, the $F_{centr} = \frac{m \cdot v^2}{r}$, where v is the velocity, m the mass of the blade and r is the radius of the circumference)

a)



b)

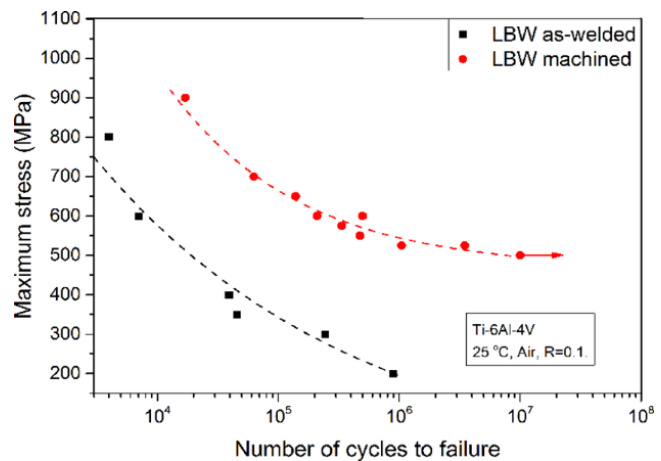


Figure 9: a) Blade dimensions and trajectory of the blade during rotation; b) S-N curves of Ti-6Al-4V samples subjected to rotating loading; both samples were laser beam welded. One sample (red curve) was machined after welding;

- Based on the S-N curves of the laser beam welded sample (no machined) in Figure 9-b, determine after how many cycles the welded blade will break. (3P)
- Why does the fatigue behavior of the blades improve after machining? (2P)

